

## Article

# Recycling Discarded Facemasks of COVID-19 Pandemic to New Novel Composite Thermal Insulation and Sound-Absorbing Materials

Khaled Al-Salem<sup>1</sup>, Mohamed Ali<sup>1,\*</sup> , Redhwan Almuzaiqer<sup>1,2</sup>, Zeyad Al-Suhaibani<sup>1</sup> and Abdullah Nuhait<sup>1</sup>

<sup>1</sup> Mechanical Engineering Department, College of Engineering, King Saud University, P.O. Box 800, Riyadh 11421, Saudi Arabia

<sup>2</sup> K.A.CARE Energy Research and Innovation Center at Riyadh, Riyadh 11421, Saudi Arabia

\* Correspondence: mali@ksu.edu.sa

**Abstract:** The COVID-19 pandemic has forced the whole world to wear single-use disposable facemasks for health protection. Studies have shown that about 129 billion facemasks are wasted each month, which will contaminate the environment and create a big problem in getting rid of them. These discarded facemasks are usually dumped in garbage bins, in landfills, or in some cases littering them on the streets, which creates a health hazard to human beings. In order to solve such environmental problems, the current study presents new novel composite materials developed by recycling discarded facemasks. These materials have great potential to be used for both thermal insulation and sound-absorbing for building walls. Experiments have been performed to make bound composite materials using the discarded facemasks as new raw materials with wood adhesive as a binder. The discarded facemasks were first heated for one and half-hour at 120 °C to kill any contaminants (biological or others). Five different composites are made: the first uses the complete facemasks, the second uses facemasks with iron nose clip only, the third uses facemasks with no both ear loops and iron nose clip, the fourth one contains the elastic ear loops only, and the fifth one has facemasks with elastic ear loops only. Coefficients of thermal conductivity for the five samples are obtained as 0.0472, 0.0519, 0.05423, 0.0619, 0.0509 (#5, e), and 0.04347 (#5, f) W/m K at 25 °C, respectively. The sound-absorbing coefficient for samples 1, 2, and 3 is above 0.5 in general and, at some frequencies, approaches 0.8. Results show that the soft samples with low binder concentration have a good sound absorbing coefficient at high frequency, while the one with high binder concentration has that at a low frequency for the same facemasks' mass. Mechanical properties of all samples are also reported by performing the three-point bending moment. Composite samples have a low moisture content (0.2%) and have high thermal stability up to 325 °C. These composite samples could replace the petrochemical and synthetic thermal insulation materials and, at the same time, get rid of the huge discarded waste facemasks, which is considered a huge environmental problem.

**Keywords:** recycling facemasks; thermal conductivity coefficient measurement; sound-absorbing coefficient; management of disposable facemasks; thermo-gravimetric analysis; scanning electron microscopy



**Citation:** Al-Salem, K.; Ali, M.; Almuzaiqer, R.; Al-Suhaibani, Z.; Nuhait, A. Recycling Discarded Facemasks of COVID-19 Pandemic to New Novel Composite Thermal Insulation and Sound-Absorbing Materials. *Sustainability* **2023**, *15*, 1475. <https://doi.org/10.3390/su15021475>

Academic Editors: Harshit Mahandra, Farzaneh Sadri and Monu Malik

Received: 30 September 2022

Revised: 4 January 2023

Accepted: 10 January 2023

Published: 12 January 2023



**Copyright:** © 2023 by the authors. Licensee MDPI, Basel, Switzerland. This article is an open access article distributed under the terms and conditions of the Creative Commons Attribution (CC BY) license (<https://creativecommons.org/licenses/by/4.0/>).

## 1. Introduction

As the COVID-19-induced emergency response is settling down around the world, the use of face masks remains the recommended action for the foreseeable future. This means that the wasted facemasks will continue to fill our waste dumps, adding to the global waste problem. In fact, it is estimated that the world discards 3 million facemasks per minute [1]. In a similar study [2], 129 billion discarded facemasks have been estimated monthly as part of personal protective equipment (PPE) during the COVID-19 pandemic, which could cause environmental contamination if not disposed of properly. Silva et al. [3] have shown that 3.5 million tons of facemasks were landfilled worldwide in 2020. They

have highlighted some innovative technologies to improve waste management of personal protective equipment (PPE). Torres and Torre [4] have reviewed the innovative management of facemask wastes during the COVID-19 pandemic. They provided a case study of Peru about the generation of facemask waste. In many cases, the facemasks end up in toxic waste bins, which adds to the cost of toxic waste handling. There have been many attempts at safe and practical ways to reuse facemasks; however, the effectiveness of those attempts is inconclusive [5]. To reuse facemasks, they need to be decontaminated first using heat. Many researchers have investigated the amount of heat needed to successfully kill off all viruses and microbes that might be left in the mask. Côrtes et al. [6] estimated that exposing the masks to 75 °C for 45 min was enough for successful decontamination. The National Health Commission of China [7] stated that 56 °C for 30 min was enough to inactivate the remnants of the COVID-19 virus. Wang et al. [8] suggested that 56 °C is enough for decontamination if masks are soaked in water at 56 °C or higher for 30 min. All of the aforementioned suggestions for decontamination costs a considerable amount of energy to accomplish. However, it was shown by Abraham et al. [9] that decontamination can be conducted with much less energy. They have shown that at 75 °C, it only takes 3 min to decontaminate the masks. The time needed for decontamination increases almost exponentially as the temperature decreases. After decontamination, the masks can be reused safely. Saberian et al. [10] suggested adding shredded facemasks to recycled concrete. They found that the added masks increased the compressive strength of the concrete. Koniarczyk et al. [11] have recycled facemasks into a concrete mixture. Their results indicated that the addition of facemasks into concrete did not deteriorate its properties but increased the compressive strength by 5% and decreased the tensile strength by 3%. A similar study has been performed by [12]. Rehman and Khalid [13] found improved strength characteristics of clay when the soil is treated with facemask fibers. A similar outcome was found by Lynch et al. [14]. A review study was carried out by Asim et al. [15] on waste management related to waste valorization of discarded facemasks since they presented the major type of waste during the COVID-19 pandemic. Microplastic pollution, due to the extensive use of facemasks, was investigated by Ray et al. [16] in an attempt to prevent polluting aquatic environments. An innovative way to manage the waste facemasks was presented by [17], where co-carbonization of disposable face masks and Daniella Oliveri leaves were performed to develop hybrid biochar. Abdullah and Abd El Aal [18] have reused healthy personal protective materials during the COVID-19 pandemic, including facemasks, in enhancing the geotechnical properties of Najran's soil for road construction in Saudi Arabia. Chen et al. [19] have shown that disposable facemasks are significant sources of micro plastics to the environment. In their study, they evaluated the ability of disposable facemasks to release micro plastics into the water. Ali et al. [20] suggested the novel use of facemasks as insulation material. They performed thermal conductivity and sound-absorbing measurements for melted and loose facemasks. They found that the melted and loose masks could make a cheap and effective insulation material.

The objective of the present study is to introduce a new management method for discarded facemasks in order to lower the environmental impact. Therefore, new resin-bound composite thermal insulation and sound-absorbing materials were developed from such discarded facemasks in order to propose the addition of value and return to one part (facemasks) of the personal protective equipment (PPE) production chain for the health sector.

## 2. Materials, Methods, and Tests

### 2.1. Collecting and Preparing the Discarded Facemasks

Used facemasks are collected by our research team such that each research team's household collects its used facemasks and bring them to the laboratory instead of discarding them in the trash. The collected discarded facemasks are oven heated at 120 °C for one and half-hour to simulate the viral disinfection. It should be noted that all precautions must be taken when handling the collected discarded facemasks. The collected facemasks

are of single-use three-layer components ear loop type as seen in Figure 1a,b. Figure 1c,d shows the convection oven used for viral disinfection. More details about the three-layer components of loose facemasks can be found in our previous publication [20].

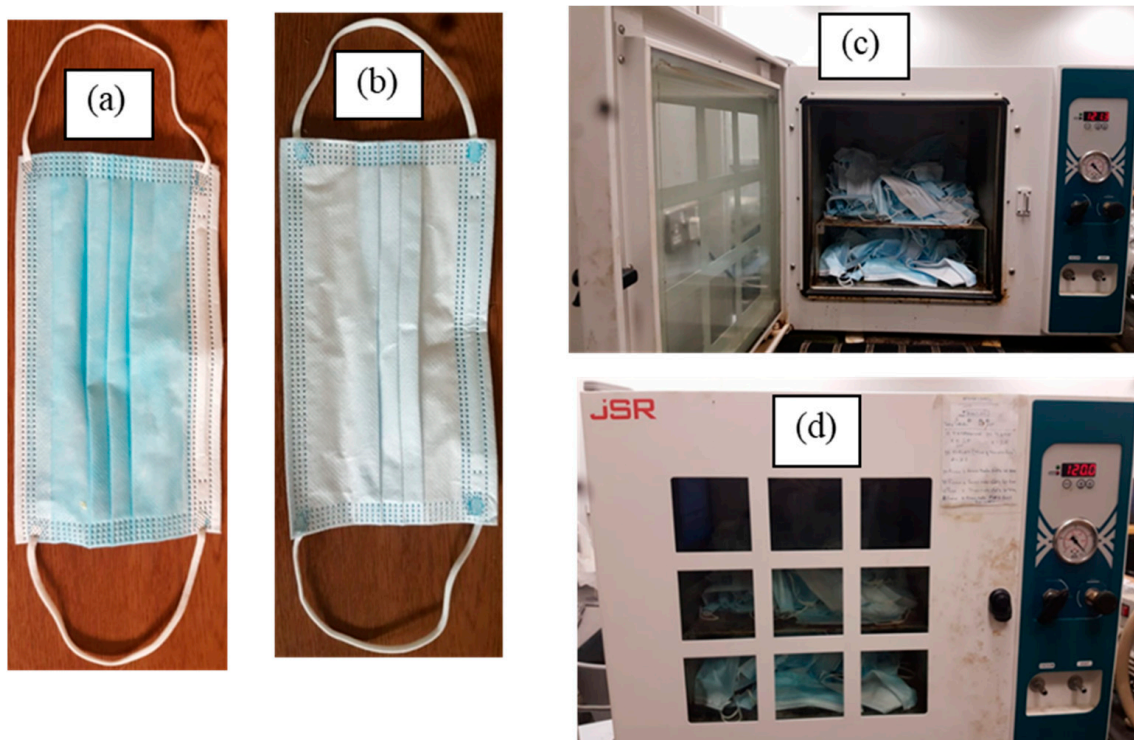


**Figure 1.** Used facemasks (a,b) and the convection oven (c,d) used for viral disinfection.

## 2.2. Preparing the Bound Facemasks' Samples

The wood adhesive is used as a binder for the facemasks. Table 1 shows the physical properties and the technical data for the wood adhesive as provided by the manufacturer. Water is added to the wood adhesive to make a solution, which is used to bind the facemasks. Each facemask is painted with the binder solution from both sides using a brush and arranged in the mold, and then it moves to the presser, followed by the convection oven for drying at 100 °C. After that, the sample is moved to the heat flow meter for thermal conductivity coefficient measurement. Figure 2 summarizes the sample preparation steps. It should be noted that wood adhesive has proved to be an effective good binder in making thermal insulation boards [21–23]. Five different bound samples are made and shown in Figure 3. Table 2 shows the physical properties, dimensions of each sample, the density, the percent of dried polymerized binder, binder mass, and the total mass of each sample. It should be noted that sample # 5 (e, f) is made using the same mass of dry facemasks (289 g) but using a different binder mass in order to see the effect of polymerized binder on the value of the thermal conductivity coefficient.

**Table 1.** Wood adhesive (78-1040)'s technical data as provided by the manufacturer [24].

Ingredients		
Name	Case-No.	Content %
Polyvinyl Acetate	9003-20-7	77–85
Water	1132-18-58	5–10
Dibutyl phthalate (DBP)	84-74-2	1–3
Calcium Carbonate	1317-65-3	10-20

Table 1. Cont.

Ingredients			
Physical and Chemical Properties			
Base material	Polyvinyl Acetate	Coverage (Approx.)	4–5 m <sup>3</sup> /kg, depends on the surfaces
Color	Milky white	Application temperature	5 °C–50 °C
Viscosity at 25 °C, ASTM D2196	25,000–34,000 CPS (Sp.# 7 at 20 rpm)	Drying time	30 min to approx 1 h. (depends on the thickness of the adhesive layer, kind of wood, and climatic condition)
Density	1.10–1.5 g/cm <sup>3</sup>	Open time	1–5 min (depends on climatic condition)
PH, ASTM D 1172	6.5–8	Full cure	24 h (depends on climatic condition)
Solid contents, ASTM D 1644	51–56%	Pressing time	12 h (depends on climatic condition and wood type)

Table 2. Composite facemasks’ properties for fixed sample size of 0.3 × 0.3 m<sup>2</sup>.

	Bound Samples Number					
	1	2	3	4	5	
	Complete Facemasks	Masks with Iron Nose Clip Only	Masks with No Ear Loops and Iron Nose Clip	Elastic Ear Loops Only	Masks with Elastic Ear Loops Only	
Material						
Figure No.	Figure 3a	Figure 3b	Figure 3c	Figure 3d	Figure 3e	Figure 3f
Total mass, g	460	562	542	298	557	400
Masks’ mass, g	314	289	291	203	289	289
Number of used facemasks	103	116	125	372	100	100
Binder’s mass, g	146	273	251	95	268	111
Percent of polymerized binder to total mass	31.7%	48.6%	46.3%	31.9%	48.1%	27.8%
Thickness, m	0.021	0.024	0.022	0.018	0.024	0.025
Density, kg/m <sup>3</sup>	243.4	260.2	273.7	184.0	257.9	177.8
Symbol	●	■	◆	▲	□	◇

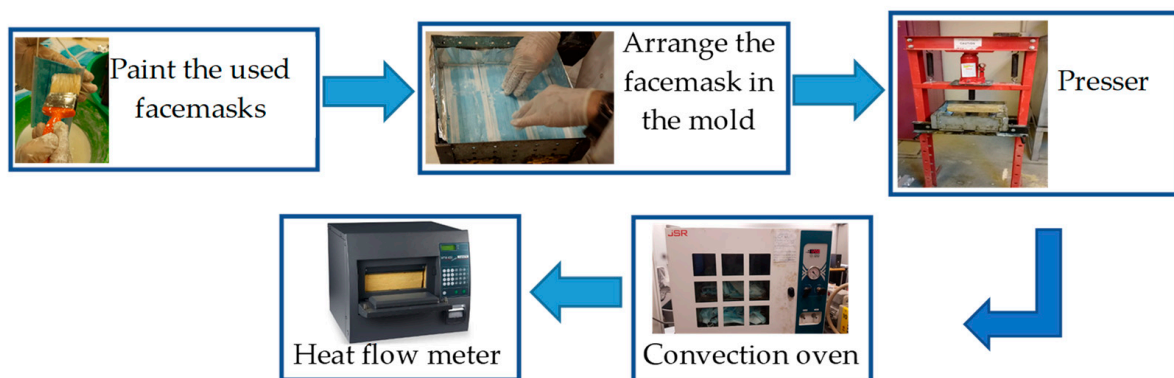
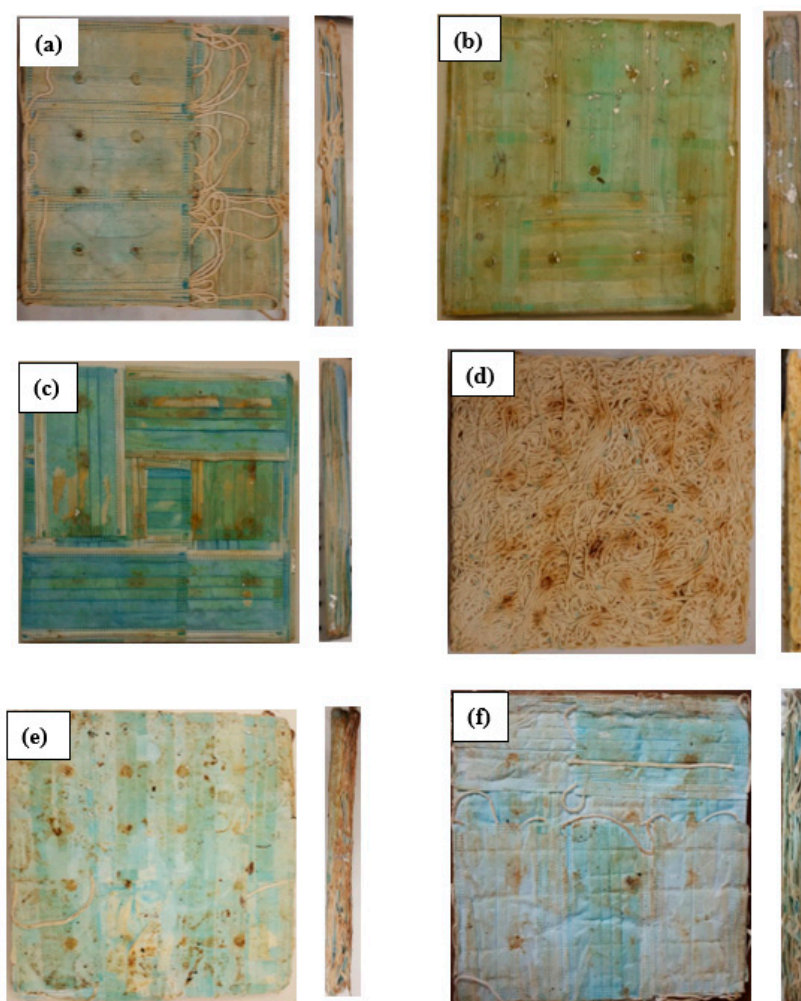


Figure 2. Bound composite sample preparation steps for thermal conductivity measurement.



**Figure 3.** Bound facemask samples: (a) complete facemasks, (b) facemasks with only iron-nose clip, (c) facemasks (no loops and iron nose clips), (d) only elastic loops, (e) facemasks with elastic loops only and high binder ratio (no iron-nose clip), and (f) facemasks with elastic loops only but low binder ratio.

### 2.3. Microstructure Analysis of the Composite Samples

Bound composite facemask samples are characterized by applying scanning electron microscopy (SEM) and the energy-dispersive X-ray (EDS) spectroscopy analysis.

#### 2.3.1. Scanning Electron Microscopy (SEM) Analysis

A small mass of composite sample 1 is used at different magnifications to determine its surface morphology. The surface morphology and chemical composition of this sample were characterized by a field-emission scanning electron microscope (FE-SEM) from Jeol Company (Tokyo, Japan), model number JSM7600F, which is equipped with energy dispersive X-ray spectroscopy (EDS). The sample is coated with platinum (Pt) for 35 s (layer thickness 25 nm) to avoid sample charging under the electron beam. The secondary electrons were used for imaging. An accelerating voltage of 15 kV was used, along with a working distance of 4.5 mm. This test follows the ASTM-E1508-98 [25] Standard. The same conditions were used during the EDS analysis except for the working distance, which was 8 mm.

#### 2.3.2. Energy Dispersive X-ray Spectroscopy (EDS) Analysis

The chemical composition of the composite bound samples was obtained using the EDS analysis at different spots. It should be mentioned that this test gives qualitative results

about the composition of the bound sample. It should be mentioned that the Field Emission Scanning Electron Microscope (FE-SEM) from Jeol Company, model number JSM7600F is equipped with (EDS).

#### 2.4. Thermal Conductivity Coefficient Measurement

Samples 1, 2, 3, 4, and 5, shown in Figure 3 with complete specifications in Table 2, are moved to a bench type heat flow meter (HFM 436 Lambda, (Selb Germany)) for measuring their thermal conductivity coefficient (k). Coefficient k is measured in a temperature range of 20–80 °C. The heat flow meter is based on the hot and cold surfaces, where heat flows between them at a mean temperature difference of 20 °C. The sample with a specific size of 30 × 30 cm<sup>2</sup> and with variable thickness is enclosed between the two plates for thermal conductivity coefficient measurement. The HFM is equipped with a sensor for automated sample thickness measurement. The HFM follows the standard ASTM-C518 [26].

#### 2.5. Thermal Property Analysis

Thermogravimetric analysis (TGA), differential (DTGA), and differential scanning calorimetry (DSC) are obtained for the loose facemasks and for the composite bound sample to characterize their thermal behavior and stability. These analyses have been conducted by using the TA instrument (New Castle, DL, USA), SDT Q600 V20.9 Build 20 setup. This instrument is fitted with nitrogen purge gas. The used composite and loose facemask masses for the analyses were 5.66 mg and 4.06 mg, respectively. An Alumina pan is used to contain the sample mass during the heating up to 550 °C. The heating starts at 25 °C, at a heating rate of 10 °C/min, and a mass flow rate of 100 mL/min of nitrogen gas.

#### 2.6. Sound Absorption Coefficient Determination

The sound absorption coefficient is measured using an impedance tube provided by BSWA Technology Ltd. (Beijing, China) at a wide range of frequencies. Ten- and three-centimeter diameter tubes are used for a frequency range of 400–6300 Hz. Details about the shape of the tubes with more specifications, the principle of operation, and the specific number and location of the microphones associated with each tube for measuring the sound-absorbing coefficient at a specified frequency can be obtained from our previous publication [20]. Sound absorption coefficients are obtained for samples 1, 2, 3, and 5.

#### 2.7. Bending Moment Tests of the Composite Samples

Mechanical important properties and parameters for the five composite samples (#1, 2, 3, and 5) are obtained by performing a bending test based on the three points. Bending test specimens are obtained for the corresponding samples 1, 2, 3, and 5. Figure 4a shows specimens 1, 2, and 3. The dimensions of the specimens are listed in Table 3. The bending force, deflection, flexural stress  $\sigma_f$ , and flexural strain  $\epsilon_f$  for each specimen are obtained by the Universal Testing Machine (UTM, INSTRON 5984) (Figure 4b,c) of 2 mm/min crosshead speed. Equation (1) is used to calculate the flexural elastic modulus  $E_f$ .

$$\sigma_f = \frac{3FL}{2bd^2}, \epsilon_f = \frac{6Dd}{L^2}, E_f = \frac{L^3S}{4bd^3} \quad (1)$$

where  $d$ ,  $b$ ,  $L$ , and  $S$  stand for thickness, width, span length of the specimen (Figure 4a), and the slope, respectively. The Universal Testing Machine reports the deflection  $D$  at the specimen's center and the associated load  $F$ . The straight-line portion of the force-deflection profile is used to determine the slope  $S$ . This test follows the standard ASTM D790-03 [27].

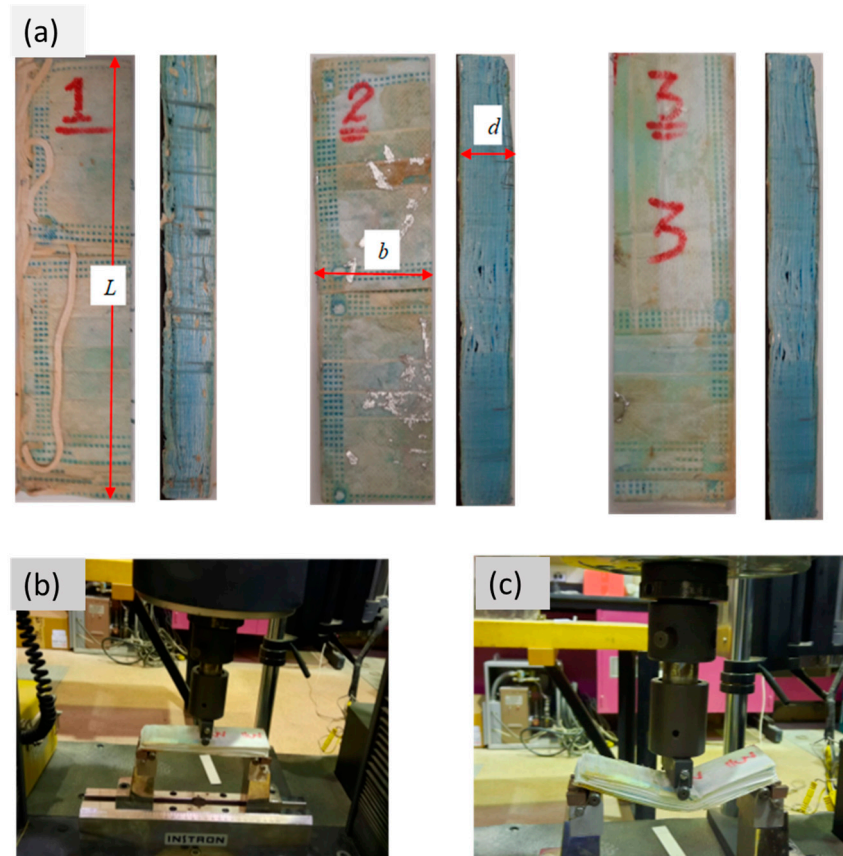


**Figure 4.** Three-point bending test (a) Specimens and (b,c) the used Universal Testing Machine.

**Table 3.** Dimensions of bending bound specimens of samples 1, 2, 3, and 5.

Bound Samples	Thickness $d$ (mm)	Width $b$ (mm)	Span $L$ (mm)	Slop $S$ (N/mm)
1	21.00	54.40	150.00	2.8
2	24.00	53.30	150.00	9.4
3	22.00	52.82	150.00	12.6
5(e)	24.00	51.00	150.00	6.8
5(f)	25.00	49.00	150.00	0.26

### 2.8. Swelling and Moisture Content Tests

A small mass of 2.6416 g (a very sensitive scale with an accuracy of 0.0001 g is used) of composite sample number 1 is soaked in a beaker full of water for 24 h, as shown in Figure 5. After 24 h, the specimen's mass is traced to check if it has any swelling or not. The thickness is also checked. On the other hand, the moisture content of the specimen is determined by heating the specimen in an oven at 100 °C for 24 h, and then its mass is recorded as  $m_2$  (dry mass). After that, the specimen's mass is tracked over time until it reaches a constant mass ( $m_1$ ). This test was performed at the laboratory conditions of 22.6 °C and relative humidity of 36.7%. The percent of moisture content absorbed by the composite specimen was determined by Equation (2) following the ASTM D2974-07A [28] standard.

$$\% \text{ of moisture content} = \frac{m_1 - m_2}{m_2} \times 100 \quad (2)$$



**Figure 5.** The beaker and the composite specimen used for the swelling test.

### 3. Results and Discussion

This study investigates the thermal and acoustic properties of resin-bound composite materials developed from discarded facemasks. In addition to that, thermal stability analysis and surface morphology are obtained for the bound composites. Bending moment tests are obtained to explore the possibility of using resin-bound facemasks as a standalone insulation material for building walls. It should be noted that this research started at the beginning of 2020 and was completed in the middle of 2021.

Figure 6a,b shows the surface morphology of the bound composite sample 1 of the facemasks at two magnification spots. The polymerized binder is shown at different spots in Figure 6a, which is marked by red elliptical shapes using 600 magnification. The fiber's average diameter has a range between  $4.78\ \mu\text{m}$  and  $10.1\ \mu\text{m}$ . Figure 6b shows a clear spot away from the polymerized binder for 1000 magnification. This figure indicates that the fibers of the facemasks are porous, as expected. The morphology structure is important to clarify the tubular structure and the porosity of the facemasks. It is well known that the thermal conductivity coefficient values are highly affected by porosity. Furthermore, Figure 6b indicates the smoothness of the facemask's fibers with almost no roughness. Figure 7a–c shows the EDS analysis of the facemask's fiber at three different spots. Spot of spectrum 1 focuses on the binder contents in Figure 7a. The constituents of the binder are mainly Calcium, as expected, in addition to Carbon and Oxygen, as their percent is shown in the spectrum analysis in Figure 7a. The second spot focuses on the facemask's fibers themselves only, as shown in Figure 7b. The major constituents of the fibers are Carbon, with 83.59%, followed by Oxygen, with 8.19%, and a very small percentage of Silicon and Calcium, as shown in spectrum 2 in Figure 7b. Furthermore, the complete picture of both facemask's fibers and the polymerized binder is shown in Figure 7c. The main elements, including both fibers and the binder, are Carbon, Oxygen, and Calcium, as shown by spectrum 3 in Figure 7c. It should be noted that in order to study any material under SEM, the surface must be conductive to avoid sample charging, as mentioned earlier in Section 2.3.1. Consequently, since the surface in our case is nonconductive, the samples are coated by Pt for a certain time to achieve at least a layer thickness of 25 nm. Therefore, during the EDS analysis, the coated Pt that appeared in the pattern is neither a contamination nor a replacement.

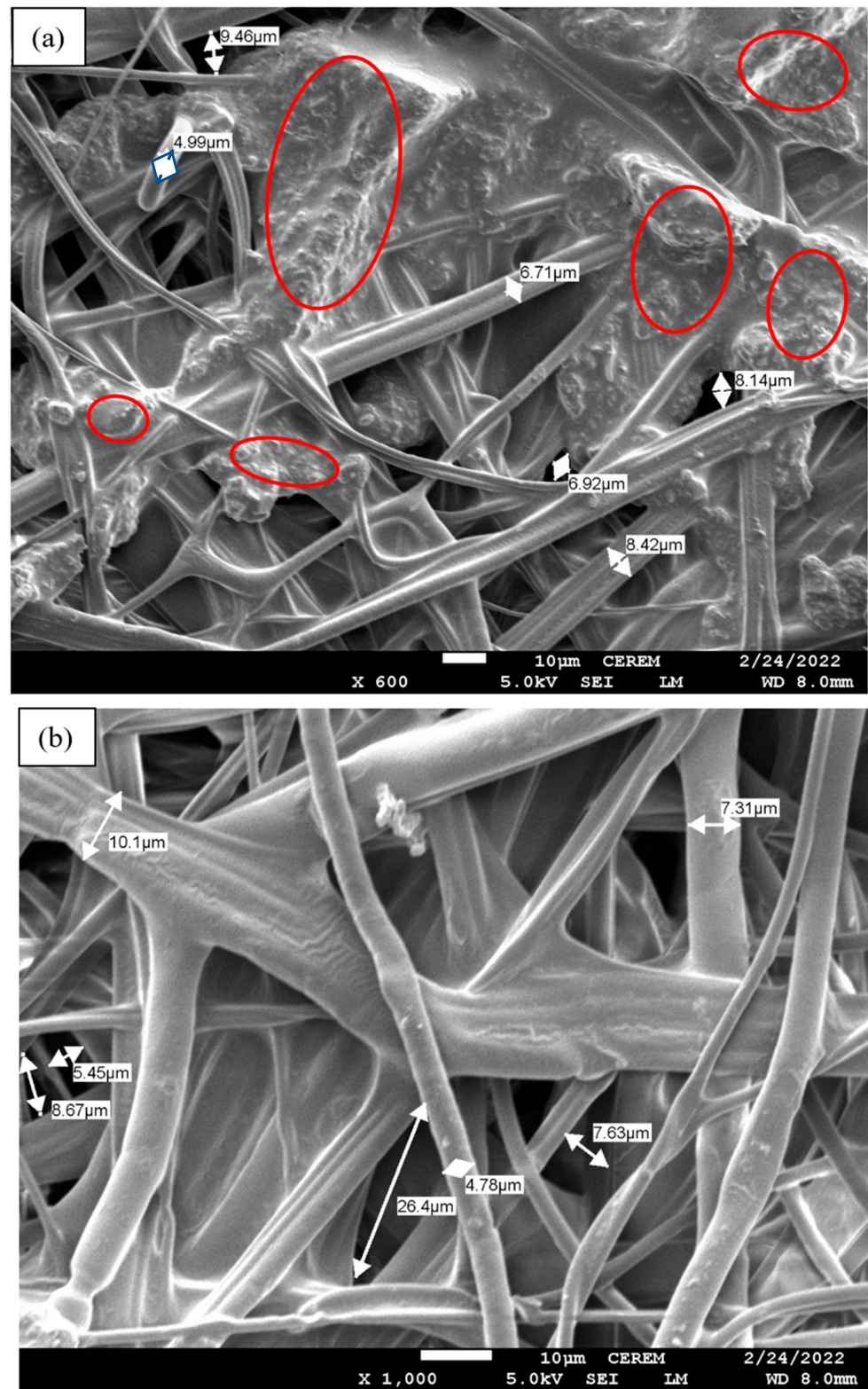


**Figure 6.** Surface morphology of the bound facemask: (a) spot showing the polymerized binder at 600 magnification and (b) clear spot at 1000 magnification.

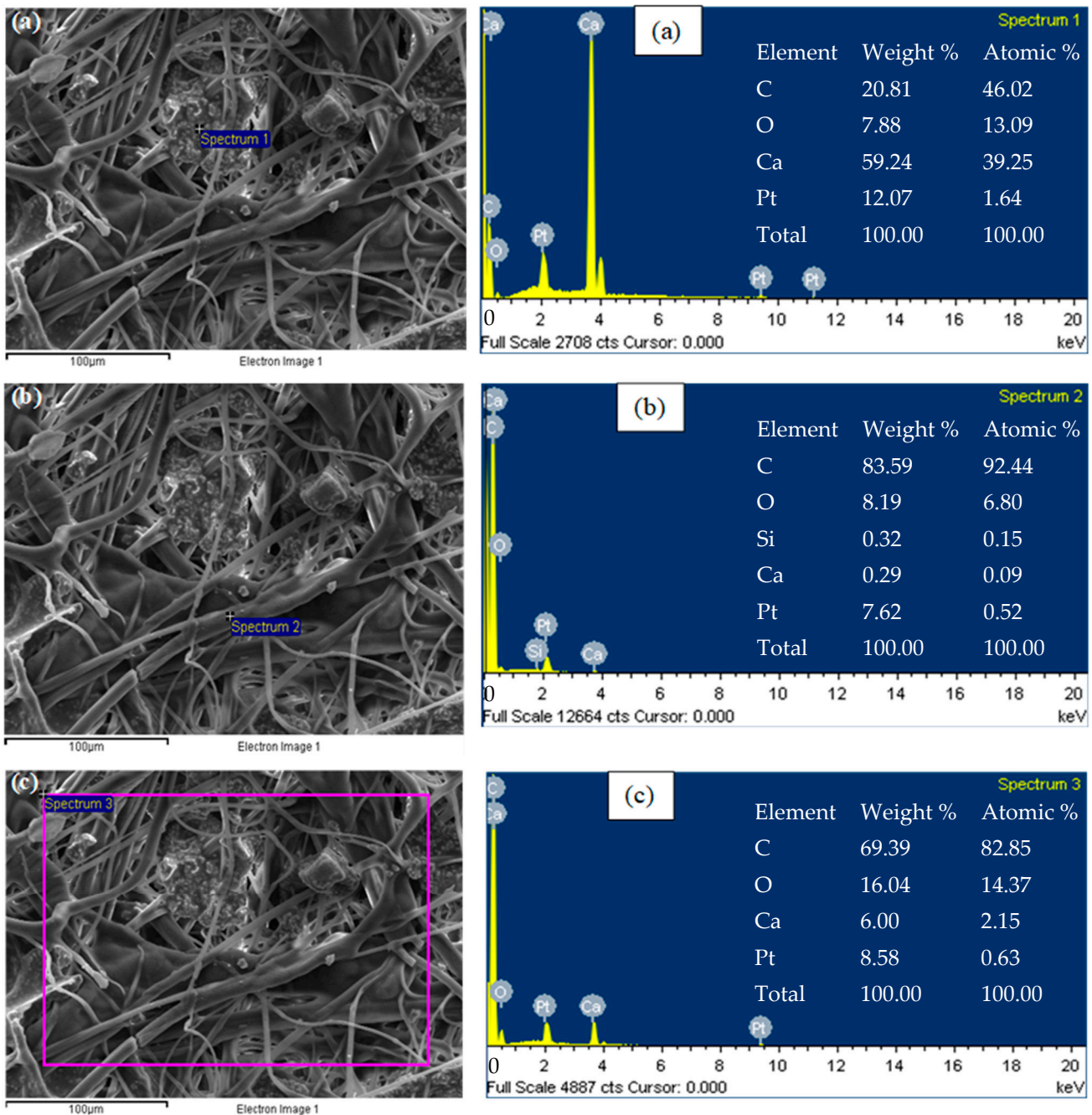


**Figure 7.** EDS analyses of the facemask’s fibers at three different spots: (a) at the polymerized binder, (b) at the fiber itself, and (c) at large spot includes both the fibers and the binder.

Figure 8 shows the thermal conductivity coefficient ( $k$ ) distribution between the temperature range 20 °C and 80 °C for bound samples compared to loose facemask sample. Complete bound facemasks (sample # 1, ●), with only iron nose clip (sample # 2, ■), facemasks with no iron nose clip and ear loops (sample # 3, ◆), elastic ear loops only (sample # 4, ▲), and facemasks with only ear loops (sample # 5, (e) □, and (f) ◇) are shown in Figure 8 compared to loose facemasks sample (+). It is clear that loose facemasks sample (+) has more porous air, which is why they have lower thermal conductivity. However, adding resin (wood adhesive) to the samples reduces the porous air, and in addition to that, the resin has different higher thermal conductivity, which tends to raise the thermal conductivity coefficient of the bound samples, as specified in Figure 8. It should be noted that removing both the nose clip and elastic ear loops (sample # 3, ◆) made the bound

sample more compact with the resin, which increases the thermal conductivity over that of loose or other bound samples (# 1, 2, and 5). To ensure that the concentration of the binder has a big role in the thermal conductivity coefficient, sample number 5 was performed twice; one with a high concentration of 48.1% ( $\square$ , sample #5(e)) and the other with 27.8% ( $\diamond$ , sample #5(f)). It is noticed that  $k$  increased by about 17.24%, corresponding to a 73% increase in the polymerized binder between sample numbers 5(f) and 5(e), as shown in Figure 8. On the other hand, elastic ear loops (# 4), which are synthetic materials (elastic polypropylene strap), give higher thermal conductivity profiles over all other samples at all temperature ranges. It is worth mentioning that at the environmental temperature of 25 °C (vertical dashed line), the thermal conductivity of all bound samples is between 0.04347 and 0.05423 W/m K, and for bound elastic ear loops, only 0.0619 W/m K. These values of the thermal conductivities promote the current new novel bound samples as new source materials for building walls' thermal insulation since the thermal conductivity is below 0.07 W/(m K). Symbols  $\star$  presents the ASTM standard with its fitting (solid line) for comparison with the other samples. Figure 8 presents the best curve fit (solid lines) to the experimental data of thermal conductivity coefficients. The correlation covering the bound and loose samples is obtained as:

$$k = A + (B \times T) \quad (3)$$

where  $k$  and  $T$  stand for thermal conductivity coefficient and the temperature in degrees Celsius. Table 4 presents  $A$ ,  $B$ , and the coefficient of determination  $R^2$  for each fit.

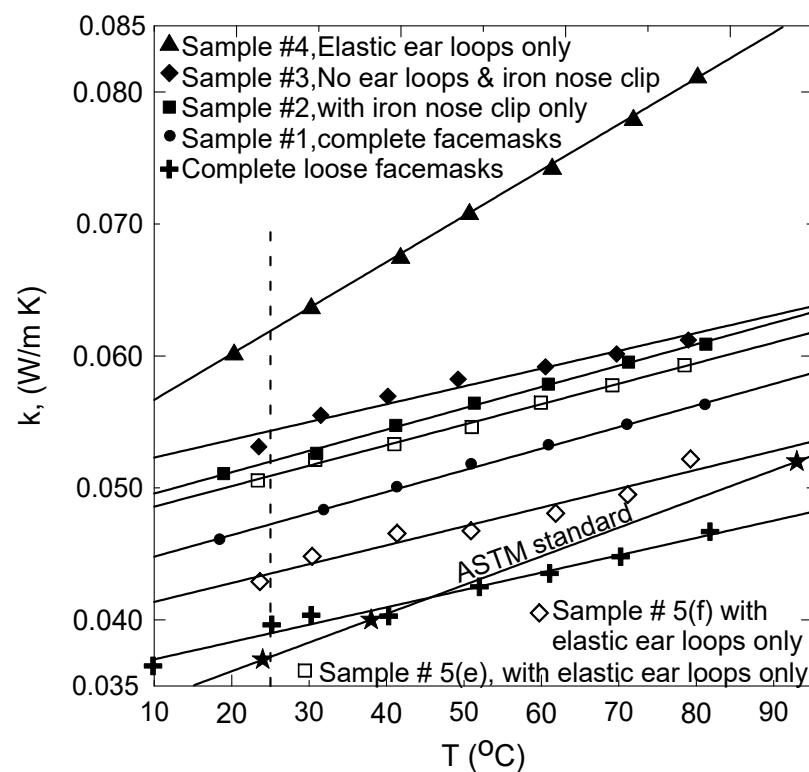


Figure 8. Thermal conductivity coefficients at temperature range of 10–80 °C for bound and loose samples.

**Table 4.** Constants presented by Equation (1) and the thermal conductivity coefficients at room temperature for different samples.

	<i>A</i>	<i>B</i>	<i>R</i> <sup>2</sup> , %	<i>k</i> at 25 °C
Sample 1, ●	0.0432	0.00016	99.8	0.0472
Sample 2, ■	0.0479	0.00016	99.7	0.0519
Sample 3, ◆	0.0509	0.000135	95.7	0.05423
Sample 4, ▲	0.0532	0.000348	99.9	0.0619
Sample 5(e), □	0.0470	0.000155	99.6	0.0509
Sample 5(f), ◇	0.0399	0.000143	94.8	0.04347
Loose sample, +	0.0357	0.0001314	97.7	0.03898

Table 5 shows a comparison between the currently developed thermal insulation samples and the conventional similar materials available in the literature. It is clear that the thermal conductivity coefficient of all samples is better than those of polypropylene (PP) and Polyethylene (PE) and close to the others. Figure 9 shows the density effects on the thermal conductivity coefficient of the bound samples (# 1, 2, 3, and 5) at different temperatures. It indicates that *k* is directly proportional to both the density and temperature. The thermal conductivity coefficient increases with the density by 25.4% and 20.2% along the isothermal lines *T* = 20 °C and 80 °C, respectively.

**Table 5.** Comparison between the thermal conductivity of the discarded facemask samples at 25 °C and other conventional materials.

Materials	Thermal Conductivity (W/m K)	References
Sample 1, ●	0.0472	Present study
Sample 2, ■	0.0519	Present study
Sample 3, ◆	0.05423	Present study
Sample 4, ▲	0.0619	Present study
Sample 5(e), □	0.0509	Present study
Sample 5(f), ◇	0.04347	Present study
Loose sample, +	0.03898	Present study
Rock wool	0.033–0.040	[29]
Expanded Polystyrene	0.031–0.038	[29]
Polyurethane foam	0.025–0.035	[30]
Phenol formaldehyde foam	0.035	[30]
Polypropylene (PP)	0.17	[31]
Polyethylene (PE)	0.17	[31]

The thermogravimetric analyses (TGA) profiles for composite facemask number 1 compared to that of loose facemasks are shown in Figure 10a. This figure shows that the composite and loose facemasks are stable up to about 325 °C and 366 °C, respectively. At these temperatures, both samples lose about 5% of their mass (● symbol). This reduction in mass could be attributed to the evaporation of moisture content in the samples, as observed before, for some insulation materials developed by agro-wasted fibers [32–34]. The composite sample has a major loss of mass between 325 °C (●)–487 °C (▲), where the composite reaches a char at 548 °C with 21% of its mass. On the other hand, the loose facemask has a major loss of mass between 366 °C (●)–471 °C (▲), where the char yields at about 500 °C with 0.5% of its mass. The composite and loose samples decompose to about 50% of their mass at 460 and 440 °C (■), respectively. The derivative thermogravimetric analysis (DTGA) is generated in Figure 10b to clarify the temperature degradation range and its peak for both composite and loose samples. These composite and loose materials, which are made of discarded facemasks, are thermally stable at high temperatures. Consequently, these good thermal stable characteristics would promote such materials to be used in building walls as new novel thermal insulation and could replace both petrochemical and/or synthetic industrial insulation materials. In addition to that, using such materials will save our environment and planet from the pollution of such discarded facemasks.

Differential Scanning Calorimetry (DSC) analysis is used to determine the phase transition, as shown in Figure 11 for composite bound sample 1 compared to that of the loose facemasks. The first endothermic transition for the bound sample and the loose one is at 167 °C and 171 °C, respectively. This phase transition may be due to losing some of the sample moisture content since both samples lose only one percent of their mass, as seen in Figure 10a. It was observed by [35] for thermal insulation material extracted from agro fibers that the transition phase may provide information about the evaporation, melting, or decomposition of that material, which indeed ensures that the first transition is due to evaporation of any moisture content in the measured samples. The second long peak transition occurs at 447 °C and 464 °C for loose and bound facemasks, respectively. At these decomposition peaks, the bound and loose facemasks have already lost about 54% and 60% of their mass, respectively. The DSC profiles of both loose and bound samples are similar, and the temperatures where the phase transition occurs are very close, which could mean that the effect of adding the binder is limited.

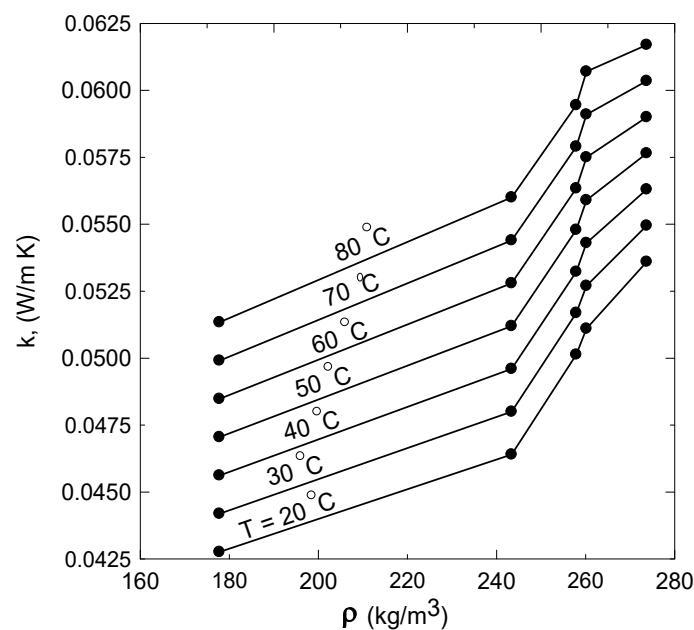


**Figure 9.** Thermal conductivity profiles versus density of bound samples number 1, 2, 3, and 5 at different temperatures.

Figure 12 embodies the sound absorption coefficient ( $\alpha$ ) profiles for the current novel bound facemasks. Sample number 1 presents the whole facemasks, where ( $\alpha$ ) approaches 0.8 at about 1600 Hz. Furthermore, ( $\alpha$ ) is above 0.5 for the frequency range 710 Hz–4750 Hz. Sample number 2 shows values  $\alpha$  above 0.5 at the high-frequency range of 2120 Hz–6000 Hz. Sample number 3 shows five peaks of sound absorption coefficients of 6.1, 6.1, 5.6, and 5.7 at frequencies 630 Hz, 1600 Hz, 2000 Hz, and 4000 Hz, respectively. These results indicate that these bound samples can be used as sound absorption materials, especially at those frequencies corresponding to the high sound absorption coefficients. Biskupicova et al. [36] have shown similar results for the sound absorption coefficient measured for ethylene–vinyl acetate and polypropylene mixture and with polystyrene and polypropylene mixture at different thicknesses with binders. Figure 13 is constructed to show the effect of polymerized binder on the sound absorption coefficient for the same facemasks' mass. Therefore, Figure 13 shows the sound absorption coefficient for sample numbers 5(e) and (f), which represent high- and low-concentrated binders, respectively. Sample 5(e) displays a bill shape at a sound absorption coefficient above 0.6 for 600–1000 Hz, where the peak of 0.86 stands at 800 Hz.

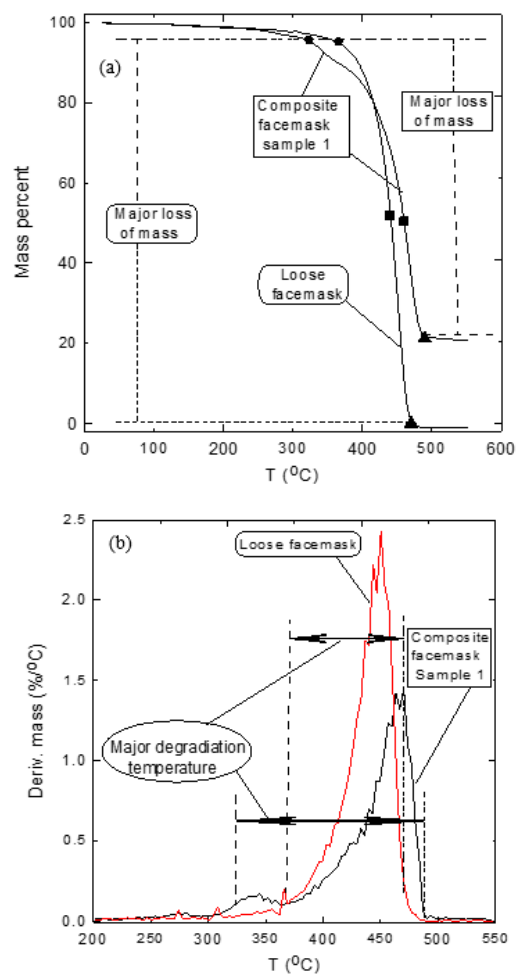


**Figure 10.** Thermal stability analysis of composite (sample 1) and loose facemasks (a) TGA profiles and (b) DTGA profiles.

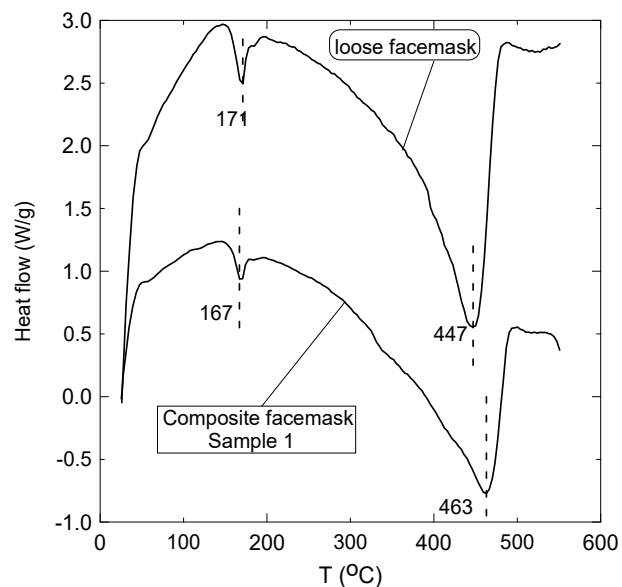


**Figure 11.** Phase transition of the composite bound sample and the loose facemask using the Differential scanning calorimetry (DSC) analysis.

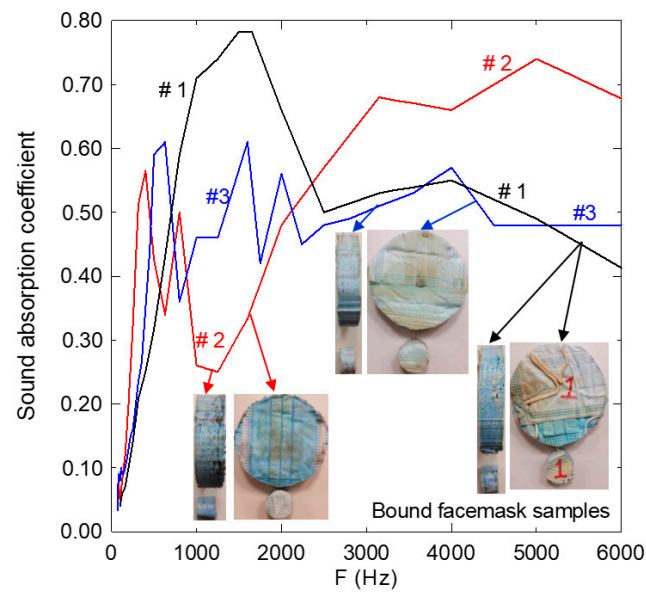


**Figure 12.** Sound absorption coefficient at various frequencies for bound samples number 1, 2, and 3.

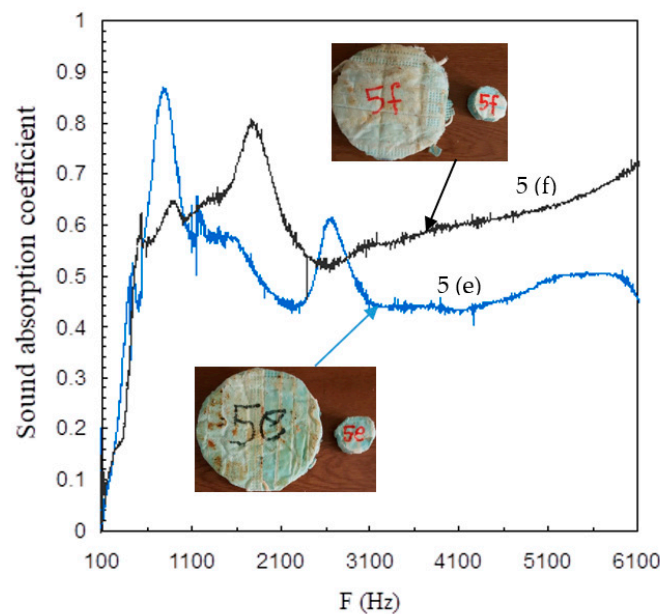


**Figure 13.** Comparison between Sound absorption coefficient at various frequencies for bound samples number 5(e) and (f).

On the other hand, sample 5(f) has a bill shape at a sound absorption coefficient above 0.6 for 800–2120 Hz, with a peak of 0.79 at 1750 Hz. Furthermore, the sound absorption increases above 0.6 for frequencies above 4000 Hz. Consequently, sample 5(f) with low binder concentration exhibits a high sound absorption coefficient at high frequency, while sample 5(e) has a good sound absorption at low frequency.

Figure 14a shows the load-deflection curves for samples 1, 2, 3, and 5(e, f). The dimensions of the specimens used for the bending test were mentioned earlier in Table 3. The slope  $S$  ( $dF/dD$ ) is obtained by the initial straight line shown in Figure 14a up to the elastic limit for the five samples. Figure 14b shows the profiles of flexural stress  $\sigma_f$  versus the flexural strain  $\epsilon_f$  for the five samples. It should be noted that both  $\sigma_f$  and  $\epsilon_f$  are calculated following Equation (1). The flexural strain  $\epsilon_f$  at maximum flexural stress is obtained from Figure 14b when the curves start to deviate from linearity [37]. Table 6 shows the maximum  $\sigma_f$  and its corresponding  $\epsilon_f$  and  $E_f$ , which is calculated following

Equation (1). Flexural modulus  $E_f$  of samples 2 and 5(e) are comparable since both have almost the same percent of polymerized binder; however, sample 1 has a lower flexural modulus  $E_f$ , since it has a lower percent of polymerized binder (31.7%). On the other hand, sample 3 is more compact since it has no ear loops and iron nose clip; therefore, it can stand higher values of  $E_f$  as shown in Table 6. Sample number 5(f) has a very low percentage of polymerized binder (27.8%); therefore, it is not strong enough (soft) and has the lowest  $E_f$  as shown in Table 6. It should be mentioned that Nguyen [38] and Dukhan [39] have indicated the improvement of  $\sigma_f$  and  $E_f$  with increasing the density of the bending specimen for aluminum foam with polypropylene, which agreed very well with these values of the present study shown in Table 6.

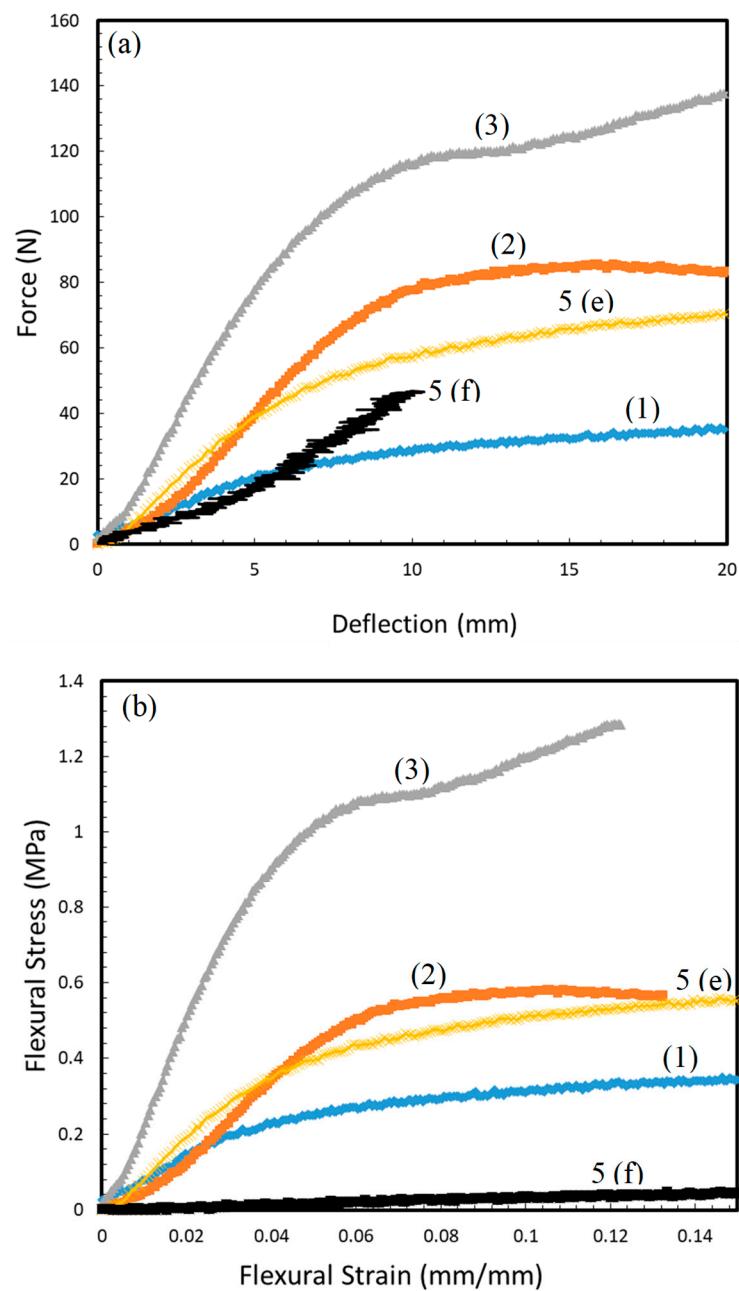


Figure 14. Bending tests for bound samples 1, 2, 3, and 5: (a) load–deflection and (b) stress–strain curves.

**Table 6.** Bending moment parameters  $E_f$ ,  $\sigma_f$ ,  $\epsilon_f$  for bound samples 1, 2, 3, and 5.

Sample Number	S (N/mm)	$E_f$ (MPa)	$\sigma_f$ (MPa)	$\epsilon_f$	Density (kg/m <sup>3</sup> )
1	2.8	4.54	0.35143	0.15423	243.4
2	9.4	9.57	0.58117	0.10504	260.2
3	12.6	20.02	1.28741	0.12200	273.7
5(e)	6.8	8.08	0.56315	0.15455	257.9
5(f)	0.26	0.286	0.07627	0.31133	177.8

Figure 15a shows that the thickness almost does not affect much before and after swelling since the increase is only 0.06 mm. However, the mass after swelling increased by almost 3 times to 7.6109 g, as shown in Figure 15b. The specimen returned to its original mass after 14 h under the laboratory conditions of 22.6 °C and 36.7% relative humidity. Figure 15c shows the tracing mass with time in hours, where the red square symbols (■) present the recorded values, and the curve fitting to the data is given by

$$\text{Mass} = 7.6068 + (0.3636 \times \text{hours}) \quad (4)$$

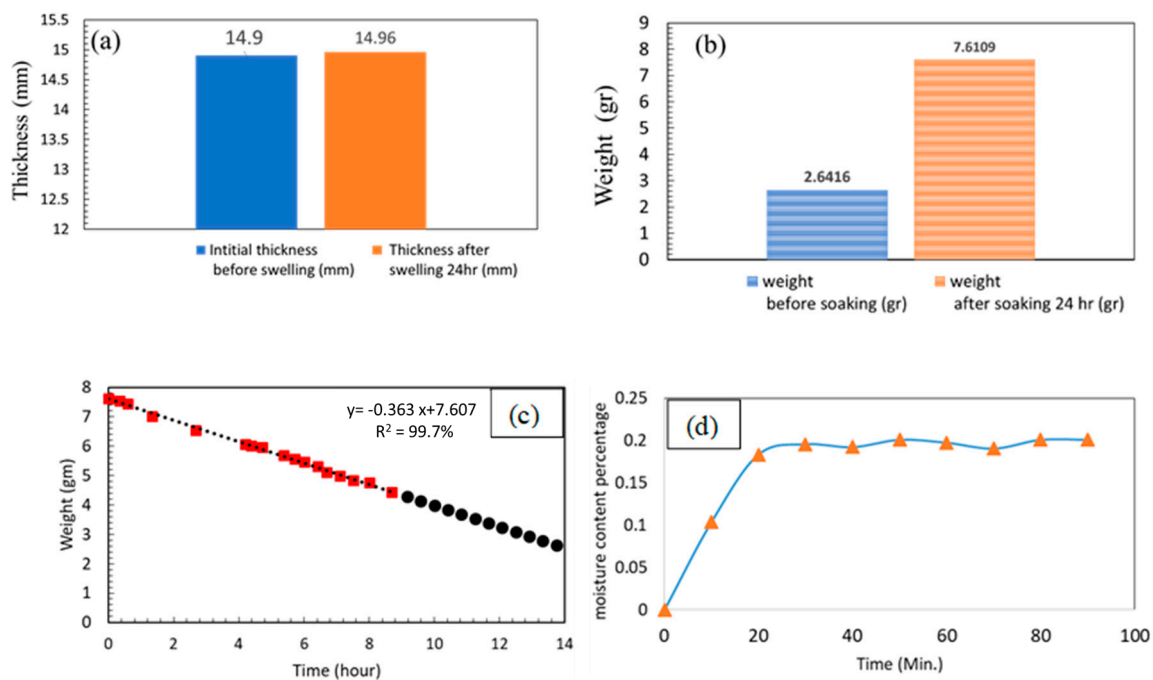


**Figure 15.** Swelling and moisture content tests: (a) thickness before and after swelling, (b) mass before and just after swelling, (c) mass tracing with time after swelling, and (d) moisture content of the composite.

With a 99.7% coefficient of determination ( $R^2$ ). The circular black symbol (●) shows the extrapolation of the equation, which shows that the mass returned to its original mass almost after 14 h, which confirms the exact measurement of the mass the next day. Figure 15d shows the moisture content profile for the specimen. This profile confirms that the composite specimen absorbs a very small amount of water, where it reaches a steady state at about 0.2% under the same laboratory conditions mentioned earlier. Consequently, the present samples have good potential to be thermal insulation materials since they have a low moisture content, as recommended by [40] for straw bale fibers insulation materials.

#### 4. Conclusions

Composite new materials have developed from discarded facemasks. Those materials are characterized as a new novel promising sound-absorbing and thermal insulation for building walls. The thermal conductivity of the newly developed samples is lower than

0.07 W/(m K) at all studied temperature ranges of 20 °C–80 °C, which promotes them as thermal insulation materials. The sequential order of the samples' best performance is 5(f), 1, 5(e), 2, and 3, based on their thermal conductivity coefficient. On the other hand, the elastic ear loops sample number 4 is valid as thermal insulation material up to 40 °C only, where its thermal conductivity is below 0.07 W/(m K). The percent of the polymerized binder has a big effect on the thermal conductivity coefficient. The sound-absorbing coefficient for samples 1, 2, and 3 are above 0.5 in general and, at some frequencies, approaches 0.8 (sample 1 at 1600 Hz). Sample 5(f) has a good acoustic characterization at high frequency, while sample 5(e) has it at low frequency. The composite samples have a high thermal stability temperature of 325 °C. Furthermore, they have a very low moisture content of 0.2%. Moreover, the composite samples 1, 2, 3, and sample 5(e) can stand high values of Flexure Modulus, as shown in Table 5. Therefore, these bound composite samples have great potential to be used as sound-absorbing and thermal insulation in building walls. In addition to that, using such discarded facemasks for developing these new novel materials will lower the environmental impact and solve the pollution problem of such waste facemasks.

**Author Contributions:** Conceptualization, M.A. and R.A.; Methodology, K.A.-S., M.A., R.A., Z.A.-S. and A.N.; Validation, R.A.; Formal analysis, K.A.-S., M.A., Z.A.-S. and A.N.; Investigation, Z.A.-S. and A.N.; Resources, M.A.; Data curation, K.A.-S., R.A., Z.A.-S. and A.N.; Writing—original draft, M.A.; Writing—review & editing, K.A.-S., M.A. and Z.A.-S.; Supervision, M.A.; Project administration, M.A. All authors have read and agreed to the published version of the manuscript.

**Funding:** The authors extend their appreciation to the Deputyship for Research & Innovation, Ministry of Education in Saudi Arabia, for funding this research work through project no. (IFKSURG-02-050).

**Data Availability Statement:** Data will be available upon request.

**Conflicts of Interest:** The authors declare that there is no conflict of interest.

## References

- Xu, E.G.; Ren, Z.J. Preventing masks from becoming the next plastic problem. *Front. Environ. Sci. Eng.* **2021**, *15*, 125. [CrossRef] [PubMed]
- Prata, J.C.; Silva, A.L.; Walker, T.R.; Duarte, A.C.; Rocha-Santos, T. COVID-19 pandemic repercussions on the use and management of plastics. *Environ. Sci. Technol.* **2020**, *54*, 7760–7765. [CrossRef]
- Silva, A.L.P.; Prata, J.C.; Duarte, A.C.; Barcelò, D.; Rocha-Santos, T. An urgent call to think globally and act locally on landfill disposable plastics under and after covid-19 pandemic: Pollution prevention and technological (Bio) remediation solutions. *Chem. Eng. J.* **2021**, *426*, 131201. [CrossRef] [PubMed]
- Torres, F.G.; De-la-Torre, G.E. Face mask waste generation and management during the COVID-19 pandemic: An overview and the Peruvian case. *Sci. Total Environ.* **2021**, *786*, 147628. [CrossRef]
- Zorko, D.J.; Gertsman, S.; O'Hearn, K.; Timmerman, N.; Ambu-Ali, N.; Dinh, T.; Sampson, M.; Sikora, L.; McNally, J.D.; Choong, K. Decontamination interventions for the reuse of surgical mask personal protective equipment: A systematic review. *J. Hosp. Infect.* **2020**, *106*, 283–294. [CrossRef]
- Côrtes, M.F.; Espinoza, E.P.S.; Noguera, S.L.V.; Silva, A.A.; de Medeiros, M.E.S.A.; Boas, L.S.V.; Ferreira, N.E.; Tozetto-Mendoza, T.R.; Morais, F.G.; de Queiroz, R.S. Decontamination and re-use of surgical masks and respirators during the COVID-19 pandemic. *Int. J. Infect. Dis.* **2021**, *104*, 320–328. [CrossRef] [PubMed]
- National Health Commission of the People's Republic of China. *Prevention and Control Program of COVID-19*, 4th ed.; General Office of National Health Commission of the People's Republic of China: Beijing, China, 2020. Available online: <http://www.nhc.gov.cn/jkj/s3577/202002/573340613ab243b3a7f61df260551dd4/files/c791e5a7ea5149f680fdb34dac0f54e.pdf> (accessed on 1 May 2020).
- Wang, D.; Sun, B.-C.; Wang, J.-X.; Zhou, Y.-Y.; Chen, Z.-W.; Fang, Y.; Yue, W.-H.; Liu, S.-M.; Liu, K.-Y.; Zeng, X.-F. Can masks be reused after hot water decontamination during the COVID-19 pandemic? *Engineering* **2020**, *6*, 1115–1121. [CrossRef]
- Abraham, J.P.; Plourde, B.D.; Cheng, L. Using heat to kill SARS-CoV-2. *Rev. Med. Virol.* **2020**, *30*, e2115. [CrossRef] [PubMed]
- Saberian, M.; Li, J.; Kilmartin-Lynch, S.; Boroujeni, M. Repurposing of COVID-19 single-use face masks for pavements base/subbase. *Sci. Total Environ.* **2021**, *769*, 145527. [CrossRef]
- Koniorczyk, M.; Bednarska, D.; Masek, A.; Cichosz, S. Performance of concrete containing recycled masks used for personal protection during coronavirus pandemic. *Constr. Build. Mater.* **2022**, *324*, 126712. [CrossRef]
- Ali, M.; Opulencia, M.J.C.; Chandra, T.; Chandra, S.; Muda, I.; Dias, R.; Chetthamrongchai, P.; Jalil, A.T. An environmentally friendly solution for waste facial masks recycled in construction materials. *Sustainability* **2022**, *14*, 8739. [CrossRef]

13. ur Rehman, Z.; Khalid, U. Reuse of COVID-19 face mask for the amelioration of mechanical properties of fat clay: A novel solution to an emerging waste problem. *Sci. Total Environ.* **2021**, *794*, 148746. [CrossRef]
14. Kilmartin-Lynch, S.; Saberian, M.; Li, J.; Roychand, R.; Zhang, G. Preliminary evaluation of the feasibility of using polypropylene fibres from COVID-19 single-use face masks to improve the mechanical properties of concrete. *J. Clean. Prod.* **2021**, *296*, 126460. [CrossRef]
15. Asim, N.; Badiei, M.; Sopian, K. Review of the valorization options for the proper disposal of face masks during the COVID-19 pandemic. *Environ. Technol. Innov.* **2021**, *23*, 101797. [CrossRef]
16. Ray, S.S.; Lee, H.K.; Huyen, D.T.T.; Chen, S.-S.; Kwon, Y.-N. Microplastics waste in environment: A perspective on recycling issues from PPE kits and face masks during the COVID-19 pandemic. *Environ. Technol. Innov.* **2022**, *26*, 102290. [CrossRef] [PubMed]
17. Emenike, E.C.; Iwuzor, K.O.; Agbana, S.A.; Otoikhian, K.S.; Adeniyi, A.G. Efficient recycling of disposable face masks via co-carbonization with waste biomass: A pathway to a cleaner environment. *Clean. Environ. Syst.* **2022**, *6*, 100094. [CrossRef]
18. Abdullah, G.M.; Abd El Aal, A. Assessment of the reuse of Covid-19 healthy personal protective materials in enhancing geotechnical properties of Najran's soil for road construction: Numerical and experimental study. *J. Clean. Prod.* **2021**, *320*, 128772. [CrossRef] [PubMed]
19. Chen, X.; Chen, X.; Liu, Q.; Zhao, Q.; Xiong, X.; Wu, C. Used disposable face masks are significant sources of microplastics to environment. *Environ. Pollut.* **2021**, *285*, 117485. [CrossRef]
20. Ali, M.; Almuzaiqer, R.; Al-Salem, K.; Alabdulkarem, A.; Nuhait, A. New novel thermal insulation and sound-absorbing materials from discarded facemasks of COVID-19 pandemic. *Sci. Rep.* **2021**, *11*, 23240. [CrossRef]
21. Owodunni, A.A.; Lamaming, J.; Hashim, R.; Taiwo, O.F.A.; Hussin, M.H.; Mohamad Kassim, M.H.; Bustami, Y.; Sulaiman, O.; Amini, M.H.M.; Hiziroglu, S. Adhesive application on particleboard from natural fibers: A review. *Polym. Compos.* **2020**, *41*, 4448–4460. [CrossRef]
22. Ali, M.; Alabdulkarem, A.; Nuhait, A.; Al-Salem, K.; Iannace, G.; Almuzaiqer, R. Characteristics of agro waste fibers as new thermal insulation and sound absorbing materials: Hybrid of date palm tree leaves and wheat straw fibers. *J. Nat. Fibers* **2022**, *19*, 6576–6594. [CrossRef]
23. Alabdulkarem, A.; Ali, M.; Iannace, G.; Sadek, S.; Almuzaiqer, R. Thermal analysis, microstructure and acoustic characteristics of some hybrid natural insulating materials. *Constr. Build. Mater.* **2018**, *187*, 185–196. [CrossRef]
24. Wood Adhesive 78-1040-Material Safety Data Sheet. Available online: <https://www.gulfindustrialgroup.com/saaf/wp-content/uploads/2016/08/WOOD-ADHESIVE-78-1040-MSDS.pdf> (accessed on 17 December 2022).
25. ASTM-E1508-98; Standard Guide for Quantitative Analysis by Energy-Dispersive Spectroscopy. ASTM: West Conshohocken, PA, USA, 2008. Available online: [www.astm.org](http://www.astm.org) (accessed on 17 December 2022).
26. ASTM-C518; Standard Test Method for Steady-State Thermal Transmission Properties by Means of the Heat Flow Meter Apparatus (C 518). American Society of Testing and Materials (ASTM): West Conshohocken, PA, USA, 2021.
27. ASTM D790-03; Standard Test Methods for Flexural Properties of Unreinforced and Reinforced Plastics and Electrical Insulating Materials. ASTM International: West Conshohocken, PA, USA, 2003. Available online: [www.astm.org](http://www.astm.org) (accessed on 17 December 2022).
28. ASTM-D2974-07A; Standard Test Methods for Moisture, Ash, and Organic Matter of Peat and Other Organic Soils. ASTM International: West Conshohocken, PA, USA, 2007. Available online: [www.astm.org](http://www.astm.org) (accessed on 17 December 2022).
29. Asdrubali, F.; D'Alessandro, F.; Schiavoni, S. A review of unconventional sustainable building insulation materials. *Sustain. Mater. Technol.* **2015**, *4*, 1–17. [CrossRef]
30. Andrady, A.L.; Neal, M.A. Applications and societal benefits of plastics. *Philos. Trans. R. Soc. B Biol. Sci.* **2009**, *364*, 1977–1984. [CrossRef] [PubMed]
31. Maddah, H.A. Polypropylene as a promising plastic: A review. *Am. J. Polym. Sci* **2016**, *6*, 1–11.
32. Marichelvam, M.; Jawaid, M.; Asim, M. Corn and rice starch-based bio-plastics as alternative packaging materials. *Fibers* **2019**, *7*, 32. [CrossRef]
33. Asim, M.; Paridah, M.T.; Chandrasekar, M.; Shahroze, R.M.; Jawaid, M.; Nasir, M.; Siakeng, R. Thermal stability of natural fibers and their polymer composites. *Iran. Polym. J.* **2020**, *29*, 625–648. [CrossRef]
34. Shahroze, R.M.; Ishak, M.R.; Salit, M.S.; Leman, Z.; Chandrasekar, M.; Munawar, N.S.; Asim, M. Sugar palm fiber/polyester nanocomposites: Influence of adding nanoclay fillers on thermal, dynamic mechanical, and physical properties. *J. Vinyl Addit. Technol.* **2020**, *26*, 236–243. [CrossRef]
35. Ball, R.; McIntosh, A.; Brindley, J. Feedback processes in cellulose thermal decomposition: Implications for fire-retarding strategies and treatments. *Combust. Theory Model.* **2004**, *8*, 281. [CrossRef]
36. Biskupičová, A.; Ledererová, M.; Unčik, S.; Glorieux, C.; Rychtáriková, M. Sound absorption properties of materials based on recycled plastic granule mixtures. *Slovak J. Civ. Eng.* **2021**, *29*, 15–19. [CrossRef]
37. RILEM-TC. Test for the determination of modulus of rupture and limit of proportionality of thin fibre reinforced cement sections. In *RILEM Technical Recommendations for the Testing and Use of Construction Materials*; CRC Press: Boca Raton, FL, USA, 1994.
38. Nguyen, D.M.; Grillet, A.-C.; Diep, T.M.H.; Bui, Q.B.; Woloszyn, M. Influence of thermo-pressing conditions on insulation materials from bamboo fibers and proteins based bone glue. *Ind. Crops Prod.* **2018**, *111*, 834–845. [CrossRef]

39. Dukhan, N.; Rayess, N.; Hadley, J. Characterization of aluminum foam–polypropylene interpenetrating phase composites: Flexural test results. *Mech. Mater.* **2010**, *42*, 134–141. [[CrossRef](#)]
40. Bainbridge, D.A. High performance low cost buildings of straw. *Agric. Ecosyst. Environ.* **1986**, *16*, 281–284. [[CrossRef](#)]

**Disclaimer/Publisher’s Note:** The statements, opinions and data contained in all publications are solely those of the individual author(s) and contributor(s) and not of MDPI and/or the editor(s). MDPI and/or the editor(s) disclaim responsibility for any injury to people or property resulting from any ideas, methods, instructions or products referred to in the content.